BxGe120/+ Clusters with x=1-4

Hung Tan Pham, [No Value]; Rizzo, Helena Girame; Havenith, Remco W. A.; Minh Tho Nguyen, [No Value]

Published in:
Journal of Physical Chemistry C

DOI:
10.1021/acs.jpcc.9b05483

Publication date:
2019

THE JOURNAL OF PHYSICAL CHEMISTRY C

Article

Cite This: J. Phys. Chem. C 2019, 123, 24676−24684

pubs.acs.org/JPCC

$B_xGe_{12}^{0/+}$ Clusters with x = 1−4: Germanium Tubes Stabilized by Three and Four Boron Dopants

Hung Tan Pham,[§,∥] Helena Girame Rizzo,[∥] Remco W. A. Havenith,[⊥,#] and Minh Tho Nguyen*[,†,‡]

[†]Computational Chemistry Research Group, Ton Duc Thang University, Ho Chi Minh City 700000, Vietnam

[‡]Faculty of Applied Sciences, Ton Duc Thang University, Ho Chi Minh City 700000, Vietnam

[§]Institute for Computational Science and Technology (ICST), Quang Trung Software Park, Ho Chi Minh City 700000, Vietnam

[∥]Department of Chemistry, KU Leuven, Celestijnenlaan 200F, Leuven B-3001, Belgium

[⊥]Zernike Institute for Advanced Materials and Stratingh Institute for Chemistry, University of Groningen, Groningen NL-9747 AG, The Netherlands

[#]Department of Inorganic and Physical Chemistry, Ghent University, Krijgslaan 281 (S3), Gent B-9000, Belgium

Supporting Information

ABSTRACT: Some boron-doped germanium clusters $B_xGe_{12}^q$ with x = 1, 2, 3, and 4 and q = 0, 1 were designed as stabilized double ring tubes. While the B_2Ge_{12} constitutes the smallest deltahedral germanium cluster, both $B_3Ge_{12}^+$ and B_4Ge_{12} clusters present us, for the first time, with an endohedral tubular motif in which either the B_3 or the B_4 cycle is encapsulated inside a Ge_{12} hexagonal prism tube. Both B_3 and B_4 units thus satisfy a geometry requirement to create an endohedral structure within the Ge_{12} double ring. Keeping their high symmetry, both B_3 and B_4 units generate delocalized bonds upon interaction with the Ge_{12} tubular framework and thereby induce an aromatic character for the resulting $B_3Ge_{12}^+$ and B_4Ge_{12}, respectively. Their aromaticity was probed by the magnetic responses of electron densities. Such a tubular aromaticity appears to greatly contribute to the high thermodynamic stability of the binary hexagonal germanium tubes.

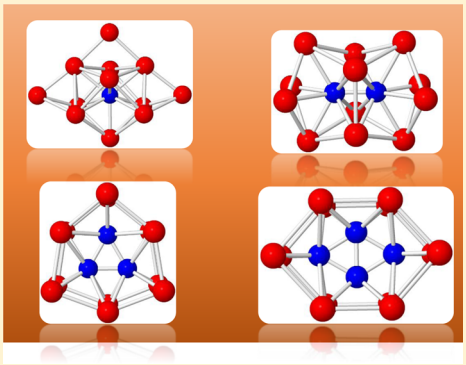

1. INTRODUCTION

Compounds based on the germanium element are used for applications in semiconductors and optoelectronic industries.[1,2] Development of new and tiny electronic devices has attracted much interest in the basic studies of the geometric, electronic, thermodynamic, and spectroscopic properties of small Ge clusters and their doped varieties.[3−13] The main objective of such investigations is a search for appropriate cluster units that can be used as building blocks for different assembly materials whose properties can effectively be controlled by a change of the cluster size and its charge as well as the nature of the dopants.

According to numerous previous investigations, the interplay between the dopants and Ge hosts controls the thermodynamic stability and provides a structural flourish for doped Ge clusters. The structural richness perspective of Ge-based clusters is clearly illustrated by, a. o., the geometry of $[M_3Ge_{18}]^q$ clusters, with M = Au, Ni, and Pd, where the Ge_{18} counterpart is actually a combination of two Ge_9 units.[14−16] Three Ni atoms generate a trimeric filament in $[Ni_3@Ge_{18}]^{4-}$, whereas Au_3 and Pd_3 each form a trimeric cycle in $[Au_3Ge_{18}]^{5-}$ and $[Pd_3Ge_{18}]^{2-}$ clusters, respectively. However, introduction of two Pd atoms to the Ge_{18} host establishes $[Pd_2@Ge_{18}]^{4-}$ as the largest single-cage deltahedron in which the Pd_2 dimer is covered by a deltahedral Ge_{18}.[17] Recently, a similar structural motif is found for $[Co_2@Ge_{16}]^{4-}$ clusters. X-ray experiments that were supported by density functional theory (DFT) computations, pointed out that $[Co_2@Ge_{16}]^{4-}$ exists in two different isomers in which both Co atoms are encapsulated by Ge_{16} cages.[18,19]

Beside such deltahedral structures, singly transition metal-doped germanium clusters provide us with a wide range of geometrical features. It is peculiar that the singly doped $CoGe_{10}^{3-}$ and $FeGe_{10}^{3-}$ clusters are stable in a double-ring tube in which either the Co or the Fe atom is centered in a D_{5h} (5/5) Ge_{10} pentagonal prism.[20,21] Another remarkable feature is the high stability of $M@Ge_{16}$ (M = Ti, Zr, and Hf) Frank−Kasper polyhedrons.[22] In the latter, a transition metal dopant is encapsulated by a Ge_{16} cage and subsequently induces a high symmetry T_d $M@Ge_{16}$. A large number of systematic investigations were carried out to elucidate the structural evolution of singly doped germanium clusters at various charged states.[23−33] Accordingly, the interplay between the metal dopant and the Ge-host gives rise to a geometrical richness which varies from incomplete cage through the encapsulated form, and then to the Frank−Kasper polyhedron.

Received: June 9, 2019
Revised: August 30, 2019
Published: September 5, 2019

DOI: 10.1021/acs.jpcc.9b05483
J. Phys. Chem. C 2019, 123, 24676−24684

Within the Ge-based garden, the doped Ge-clusters containing 12 Ge atoms emerge as the most beautiful flower owing to their typical diversity in structure and chemical bonding phenomena. A hexagonal prism shape was found for $V@Ge_{12}^-$, $Mo@Ge_{12}$, and $W@Ge_{12}$ indicating a certain similarity of germanium and silicon clusters.[30,31,34] Such an incomplete cage was identified for $M@Ge_{12}^q$ and particularly their shape is quite sensitive with respect to the charge state. Interestingly, the $AuGe_{12}^-$ anion cluster presents a high symmetry structure in which the Au dopant is encapsulated by an I_h Ge_{12} host.[35]

Recently, a hexagonal cylinder was found for the Si_{12} cluster when it is doped by three boron atoms giving the three-layer tube $B_3@Si_{12}^+$.[36,37] This result brings in an interesting possibility that small boron clusters such as B_2, B_3, and B_4 can serve as doping units in an efficient approach to generate stable tubular clusters. In this context, we set out to expand the scope of our approach in successfully stabilizing germanium clusters containing 12 Ge atoms into a hexagonal tubular prism using the effects of both boron clusters B_3 and B_4 as dopants. According to our literature survey, both the $B_3Ge_{12}^+$ and B_4Ge_{12} cases represent, for the first time, endohedral motifs in which all dopants are encapsulated within a Ge_{12} hexagonal tube. In other words, the unstable Ge double hexagonal ring tube is stabilized following doping of B_3 and B_4 units.

2. COMPUTATIONAL DETAILS

In order to construct the potential energy surfaces of $B_xGe_{12}^{0/+}$ clusters, we use a stochastic genetic algorithm developed earlier by us.[38] We now modify this algorithm by adding a permutation subroutine in which each atom exchanges its position with all the others. Moreover, to ensure that the global energy minimum isomer of each size is correctly found, several series of geometries having nonconventional shapes are also considered with the aim to search for unexpectedly stable structures. The initial structures are generated without any constrain on the largest distance of B−B, B−Ge, and Ge−Ge connectivities, whereas their shortest distances are the sum of covalence radii. We use DFT with both hybrid TPSSh and B3P86 functionals[39,40] for geometry optimizations in view of previous results that these functionals provide the reliable results.[41,42] Initial structures are first optimized using the small split-valence 3-21G basis set.[43,44] The optimized isomers, whose relative energies are lying within a range of 50 kcal/mol with respect to the lowest-lying one, are subsequently reoptimized using the same functionals, but in conjunction with the larger 6-311+G(d) basis set.[45,46] Harmonic vibrational frequencies are analyzed afterward at the same level of theory to ensure the character of the optimized structures as energy local minima and to estimate their zero-point vibrational energies. In order to explore the chemical bonding of the clusters considered, their electron density will be explored by means of the electron localization function (ELF) method,[47] Mayer bond order (MBO),[48] as well as natural bond orbital (NBO) atomic charge.[49] All standard electronic structure theory computations are performed using the Gaussian 09 suite of program.[50]

The magnetic response of the electron density is calculated using the CTOCD-DZ method[51,52] implemented in the SYSMO program,[53,54] which is connected to the GAMESS-UK package.[55] The magnetic ring current maps are then constructed using the B3P86 functional with the 6-311G(d) basis set. In each current density map, the contour and shading show the modulus of the induced current density, and the arrows display its projection on the plotting plane. As for a convention, anticlockwise or clockwise circulations of electron flows correspond to diatropic or paratropic currents, respectively. A diatropic current flow is correlated with an aromatic character, whereas a paratropic current flow suggests an anti-aromatic character.

3. RESULTS AND DISCUSSION

In the search for Ge clusters having a tubular form, we investigate the B_xGe_{12} systems in which x = 1, 2, 3, and 4. As the open-shell doublet state in both neutral BGe_{12} and B_3Ge_{12} radicals usually leads to a distorted geometry, we only report on the corresponding cations BGe_{12}^+ and $B_3Ge_{12}^+$ that exhibit a closed-shell singlet ground state. Let us first briefly report on their geometrical aspects before analyzing their electronic structure. As for a convention, structures mentioned in the following sections are denoted by **x.Y** where **x** stands for the number of B atoms, being 1, 2, 3, and 4, and **Y** = A, B, and C, ... for the isomers with increasing relative energy. Thus, structure **x.A** invariably refers to the lowest-energy isomer for the dopant B_x, and relative energy of other isomers mentioned are given, unless otherwise stated, with respect to its corresponding **A** isomer.

3.1. BGe_{12}^+. The most stable isomer **1.A** of the BGe_{12}^+ cation is given in Figure 1, whereas some of its lower-lying

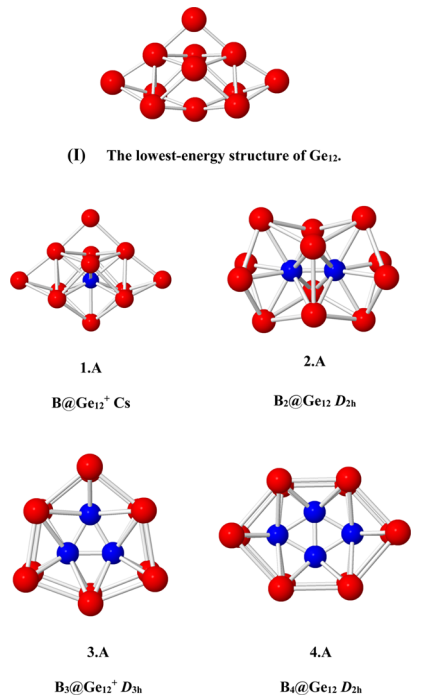

Figure 1. Geometries of Ge_{12} and $B_xGe_{12}^q$ clusters with x = 1, 2, 3, 4, and q = 0, 1. Geometry optimizations were performed using the TPSSh/6-311+G(d) and B3P86/6-311+G(d) methods.

isomers are shown in Figure S1 of the Supporting Information file. The ground state **1.A** (C_s $^1A'$) is revealed by both TPSSh and B3P86 calculations. **1.A** has an endohedral form in which the B^+ ion is covered by the most stable structure of the Ge_{12} cluster (**I**) displayed in Figure 1. Actually, a similar shape was identified for the isovalent BSi_{12}^+ in which the most stable isomer Si_{12} fully covers the B dopant.[36] Hence, the latter actually does not induce a significant modification on the geometry of both pure Ge_{12} and Si_{12} clusters.

DOI: 10.1021/acs.jpcc.9b05483
J. Phys. Chem. C 2019, 123, 24676−24684

3.2. B_2Ge_{12}. Our extensive DFT optimizations point out that a mixture of two B atoms with 12 Ge atoms induces an endohedral structure **2.A** for the neutral B_2Ge_{12}. Some lower-lying isomers are displayed in Figure S1 of the Supporting Information file. Geometric characteristics of **2.A** illustrate that both B atoms form a B−B dimer, which is encapsulated by a Ge_{12} host, then giving rise to a high symmetry D_{2h} B_2Ge_{12}. The B−B connection of **2.A**, with a bond distance of 1.73 Å, is significantly longer than that of free B_2 molecule (1.61 Å). On the one hand, formation of **2.A** reduces the strength of the B_2 molecule. For the pure Ge_{12} system, a D_{2h} isomer having the same skeleton as that in **2.A** is highly unstable on its potential energy surface.[56] An interesting finding is that the two B dopants contribute to stabilize an unstable D_{2h} Ge_{12} isomer, emphasizing a special effect of a double doping of two B atoms. According to previous reports, the geometry of the B_2Ge_{12} cluster is totally different from that of the B_2Si_{12}. As shown in Figure 2, the B_2Si_{12} is of a double ring structure in which the B_2 moiety is located inside a (6 × 2) Si_{12} prism, whereas the B_2Ge_{12} is stabilized in a deltahedral shape. This result emphasizes the different behavior between Si and Ge hosts regarding the B_2 dopant.

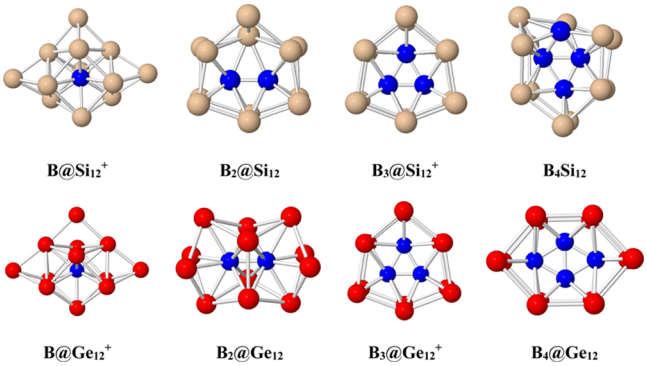

Figure 2. Summary of geometries of $[B_xSi_{12}]^{0/+}$ and $[B_xGe_{12}]^{0/+}$ clusters, with x = 1, 2, 3, 4.

Concerning the doubly doped Ge clusters having a cage shape, B_2Ge_{12} appears to be the smallest system known up to now. As mentioned above, the $[Pd_2@Ge_{18}]^{4-}$ and $[Co_2@Ge_{16}]^{4-}$ clusters are of the deltahedral germanium clusters.[17−19] According to our literature survey and own extensive computations, no size smaller than the current case of B_2Ge_{12} can form endohedral structure with two dopants. The B_2Ge_{12} **2.A** no doubt represents the smallest single deltahedron of germanium cluster which can endohedrally encapsulate two dopants. The B_2 moiety also exerts a different influence on the isovalence Si_{12} cluster which is of a C_s cage. Indeed, the most stable B_2Si_{12} is a distorted hexagonal prism in which the B_2 unit is covered by a (2 × 6) Si_{12} prism.[36,37] Hence, the B_2 dopant brings in strong modification on the geometry of both Ge_{12} and Si_{12} bare clusters. The main difference in both doped clusters is that because of its larger size, the Ge_{12} cage has more available space to fully cover the B_2 unit.

3.3. $B_3Ge_{12}^+$. Following BGe_{12}^+ and B_2Ge_{12}, the geometry of the triply boron-doped $B_3Ge_{12}^+$ with a positive charge is considered. Lower-lying isomers of the $B_3Ge_{12}^+$ cation identified by computations using both TPSSh and B3P86 functionals and the 6-311+G(d) basis set are displayed in Figure S2 of the Supporting Information file. Accordingly, isomers containing a B_3 cycle are highly stable, and among them, the structure having the highest symmetry **3.A** (D_{3h} $^1A_1'$) is found to be its ground state. **3.A** contains indeed a D_{3h} B_3 cycle which is placed inside a (6 × 2) Ge_{12} hexagonal prism, and finally establishes a D_{3h} tube. While the triatomic B_3 cycle of **3.A** is actually similar to the free B_3 cycle, the Ge_{12} counterpart is totally different from its pure ground state (C_s structure (**I**), Figure 1). Therefore, the B_3 cycle again tends to transform the geometry of Ge_{12} from a C_s cage to a D_{3h} hexagonal prism in the positively charged and singlet state. The $B_3Ge_{12}^+$ cation presents for the first time a hexagonal prism, or a double hexagonal ring tube, with three endohedral dopants for a germanium cluster, and it appears to be the smallest one of the class $M_3@Ge_{12}$. Recent reports also pointed out that a B_3 cycle exerts a similar effect on the Si_{12} host in which a D_{3h} hexagonal prism was also found as the most stable isomer for the singlet $B_3Si_{12}^+$ cation.[36] It can be concluded that the cyclic B_3 dopant consistently induces and stabilizes a tubular structure for both Si_{12} and Ge_{12} in their cationic singlet state.

3.4. B_4Ge_{12}. The geometry of the B_4Ge_{12} cluster presents us with the most interesting finding of the present work. Lower-lying isomers of the neutral B_4Ge_{12} are displayed in Figure S3 of the Supporting Information file. Similar to the $B_3Ge_{12}^+$, geometries of the B_4Ge_{12} isomers emphasize a remarkable result that the four B atoms connect together to form a B_4 cycle inside the Ge_{12} host to produce the most stable doped cluster. Both TPSSh and B3P86 calculations point out that both **4.A** (D_{2h} $^1A_{1g}$) and **4.B** (C_1 ^1A) isomers are very close in energy. However, coupled-cluster CCSD(T)/6-311G(d) calculations indicate that **4.B** actually lies ∼7 kcal/mol above **4.A**. Therefore, **4.A** is confirmed to be the most stable B_4Ge_{12} isomer.

The geometric shape of **4.A** clearly points out that a tetraatomic D_{2h} B_4 cycle is placed inside of a (2 × 6) Ge_{12} prism generating again a hexagonal prismatic shape for B_4Ge_{12}. In the pure form, a Ge_{12} tube does not exist as a local minimum. In the cationic form, it is much higher in energy in Ge_{12}^{2+} (∼30 kcal/mol) and Ge_{12}^{4+} (∼13 kcal/mol) than their corresponding global minimum Ge_{12} cages (such as **I**, Figure 1). Although the B_4 unit of **4.A** exhibits the same shape as that of the free B_4, its B−B bond length of ∼1.7 Å is actually longer than that of ∼1.5 Å in pure B_4.[57] As far as we are aware, the appearance of the **4.A** structure presents us with a particular case of doped germanium clusters, in which an encapsulation of four dopants in a double hexagonal ring tube is found for the first time.

Although a hexagonal prism form is a general structural motif for both $B_3Ge_{12}^+$ and $B_3Si_{12}^+$ clusters, this kind of structure is not found for the B_4Si_{12} cluster. Actually, the most stable structure of B_4Si_{12}, **4.Si.A** isomer, can be considered as a broken version of the B_4Ge_{12} hexagonal prism. The lower-lying isomers of the B_4Si_{12} cluster identified by the TPSSh/6-311+g(d) level of theory are given in Figure S4 (Supporting Information file). Accordingly, the **4.Si.A** isomer is found to be the lowest-energy structure, whereas the isomer **4.Si.I**, which has the same shape as that of B_4Ge_{12}, is ∼12 kcal/mol higher than **4.Si.A**. Within **4.Si.A**, boron atoms also form a B_4 cycle, but it is not planar, and one B atom replaces a Si site of the (6 × 2) Si_{12} hexagonal prism. This result emphasizes that the Si_{12} double ring is not large enough to contain a B_4 ring, whereas the Ge_{12} counterpart fits well in this geometric condition. For a complete picture, the geometries of $B_xSi_{12}^{+/0}$ and $B_xGe_{12}^{+/0}$ are shown in Figure 2.

DOI: 10.1021/acs.jpcc.9b05483
J. Phys. Chem. C 2019, 123, 24676−24684

In summary, geometric features of B_2Ge_{12}, $B_3Ge_{12}^+$, and B_4Ge_{12} clusters indicate the ability of small boron clusters to influence the geometry of the Ge_{12} moiety. While one B atom does not give a significant impact on the Ge_{12} cage, a B_2 dimer converts a C_s Ge_{12} into a higher symmetry D_{2h} shape and produces the smallest deltahedral cage for germanium clusters. The most interesting finding is that the appearance of the **3.A** and especially **4.A** clusters illustrate that both B_3 and B_4 units can be used as dopant units that strongly stabilize a Ge_{12} host into a higher symmetry hexagonal prismatic tube, forcing an adaption of the host to their point group in a suitable charge state.

Concerning the formation of prismatic germanium structures, both B_3 and B_4 units show the importance of geometry requirement. As mentioned in Introduction, three Pd or Au dopants form a Pd_3 or Au_3 triatomic cycle which connect two Ge_9 units and then generate the sandwich-type Pd_3Ge_{18} and Au_3Ge_{18} clusters. In contrast, an endohedral structure is now established with a B_3 unit.[14−16] With bond lengths of 2.9 and 3.0 Å, both Pd_3 and Au_3 cycles are apparently too large to fit inside a Ge_{18} cage, whereas both B_3 and B_4 units, with a B−B bond length of ∼1.7 Å, are more suitable for endohedral insertion. In addition, a prismatic motif was previously identified for germanium clusters doped by transition metals including a pentagonal prism for $M@Ge_{10}^q$ and a hexagonal prism for $M@Ge_{12}^q$ clusters.[21,26] Within each of these structures, the metal dopant was found to be located inside a (2×5) Ge_{10} or a (2×6) Ge_{12} prism and thereby forming $M@Ge_{10}^q$ and $M@Ge_{12}^q$ endohedral prismatic clusters, respectively. The emergence of **3.A** and **4.A** structures in which both B_3 and B_4 cycles are located inside a (2×6) Ge_{12} prism, thus provides us with a novel approach to construct endohedral prismatic structures. Generally, tubular clusters can also be established by doping a planar cluster that has a suitable size.

The high symmetry form of both $B_3Ge_{12}^+$ and B_4Ge_{12} clusters is highly suitable for the assembly materials. Upon extension of both $B_3Ge_{12}^+$ and B_4Ge_{12} hexagonal prisms along the z-axis, a novel type of nanotube is established as shown in Figure 3. Accordingly, the final forms of $[B_3Ge_{12}^+]_n$ and $[B_4Ge_{12}]_n$ nanotubes exhibit smaller $(B_3)_n$ and $(B_4)_n$ tubes covered inside the $(Ge_{12})_n$ tube. Because of the effect of $(B_3)_n$ and $(B_4)_n$ tubes, the $[B_3Ge_{12}^+]_n$ and $[B_4Ge_{12}]_n$ tubes can thus

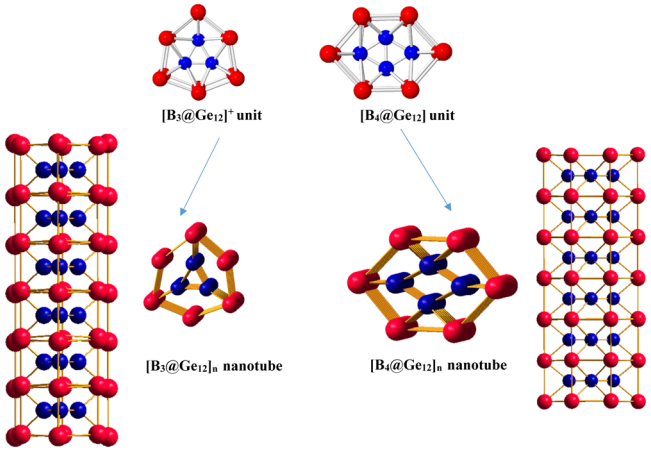

Figure 3. Formation of $[B_3@Ge_{12}]_n$ and $[B_4@Ge_{12}]_n$ assembly nanotube from $[B_3@Ge_{12}]^+$ and $[B_4@Ge_{12}]$ units.

be built up, whereas the only-Ge-based tube could not be made yet.

For a quantitative evaluation on the stability of the $[B_xGe_{12}]^{0/+}$ clusters, their binding energies are calculated and given in Table 1. Accordingly, the B_2Ge_{12} deltahedral structure and B_4Ge_{12} hexagonal prism have significantly larger E_b than that of the BGe_{12}^+ and $B_3Ge_{12}^+$ clusters. These neutral mixed clusters are in higher stability than the cations. The embedding energies, which are the energy differences between the doped cluster and the separated fragments $Ge_{12} + B_x^{0/+}$, are also performed and given in Table 1. The $B_3Ge_{12}^+$ hexagonal structure has the largest embedding energy, indicating that of the B_x dopants, introduction a B_3^+ unit into the Ge_{12} host is the most favored approach.

In attempts to understand how a B_x unit can exert such a large influence on the geometry of a Ge_{12} host, their bonding phenomenon is now explored. Investigation of electron densities of the $B_xGe_{12}^q$ clusters using the ELF points out some interesting perspectives in terms of chemical bonding. For the singly doped BGe_{12}^+ **1.A**, as shown in Figure 2, localization domains associated with B−Ge bonds are observed. However, at the bifurcation value of ELF = 0.65, in the region between B and Ge_{12} host one basin appears covering B atoms indicating the importance of the electrostatic interaction. Hence, the B^+ dopant establishes a polarized bond with Ge_{12} host. This observation is supported by NBO atomic charge calculated for the B atom which bears a value of −2.1 electron, illustrating that the Ge_{12} host actually undergoes a great charge transfer to the B center.

Concerning the smallest germanium deltahedron **2.A** of B_2Ge_{12}, two B atoms give rise to a delocalized bond with the Ge_{12} deltahedral skeleton, as indicated by ELF maps. The ELF map of **2.A** (Figure 4) shows the appearance of localization domains in regions between the B atoms and Ge_{12} host. This observation emphasizes that B dopants form delocalized bonds with the Ge_{12} counterpart. Indeed, both B dopants in **2.A** actually carry a negative NBO charge of −1.8 electron. Similar to BGe_{12}^+, Ge_{12} transfers its charge to the B_2 unit and thereby enhances its stability through the electrostatic interaction. From this view, **2.A** can be considered as a $[B_2^{\delta-}\ Ge_{12}^{\delta+}]$ donor−acceptor complex. Another important feature in B_2Ge_{12} is that both boron atoms in **2.A** connect through a covalence bond rather than existing as two separated atoms. The ELF map of **2.A** (Figure 2) also shows a V(B,B) basin located between two B atoms indicating the formation of a B−B valence bond. In addition, the MBO performed for **2.A** show a value of ∼1.0 for this B−B connection. Although this value is much lower than that of the free B_2 molecule (1.9), it suggests that the B−B moiety of B_2Ge_{12} **2.A** can be regarded as a B−B single bond.

Regarding the $B_3Ge_{12}^+$ cation **3.A**, a novel perspective on the B_3 moiety is now revealed by an ELF examination. With the appearance of a V(B,B,B) basin located over the B_3 cycle, three B atoms actually form a three-center valence bond rather than acting as three separated atoms. The MBO value calculated for the B_3 unit in **3.A** has a value of 0.44 indicating the existence of a three-center bond. In comparison to the bare $B_3^{+/-}$ clusters, the MBO value performed for these cycles amount to 1.1/0.97, being a much greater value than those of B_3 moiety of $B_3Ge_{12}^+$. Hence, according to the usual meaning of bond order, interaction with Ge_{12} to establish $B_3Ge_{12}^+$ reduces the strength of the B_3 cycle inside the Ge tube.

DOI: 10.1021/acs.jpcc.9b05483
J. Phys. Chem. C 2019, 123, 24676−24684

Table 1. Binding Energy (E_b, eV) and Dissociation Energy (E_D, eV) of $B_xGe_{12}^q$ Clusters[a]

	BGe_{12}^+	B_2Ge_{12}	$B_3Ge_{12}^+$	B_4Ge_{12}	B_2	$B_3^{-/+}$	B_4
E_b[b]	4.00/3.87	4.52/4.45	4.17/4.10	4.58/4.57			
E_D[c]	7.71/7.55	7.60/7.50	10.75/10.93	6.38/6.58			
qNBO(B)	−2.10	−1.8	−1.45	−1.30			
d (B−B)		1.73	1.76	1.70/175	1.62	1.55/1.57	1.52
MBO_{BB}		0.91	0.45	0.61/0.52	1.95	2.0/1.64	1.41
MBO_{B_x}			0.44	0.52		1.1/0.97	0.58

[a]NBO charge, bonding length of B−B connection (Å), MBO B−B connection (MBO_{BB}), MBO B_3 and B_4 cycle (MBO_{B_x}). [b]E_b values were calculated by the TPSSh/6-311+G(d) (left), and B3P86/6-311+G(d) (right). [c]This value was performed for the process: $B_xGe_{12}^q \rightarrow B_x^q + Ge_{12}$. In the reversed direction, these values correspond to the embedding energies.

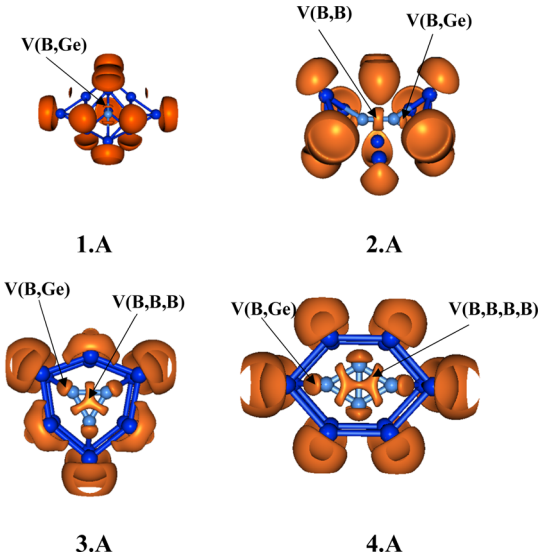

Figure 4. ELF iso-surfaces plotted at the bifurcation value ELF = 0.70 for **1.A**, **2.A**, **3.A**, and **4.A** structures. The electron density was obtained by the TPSSh/6-311+G(d) computations.

It is meaningful to consider the connection between both the B_3 cycle and Ge_{12} hexagonal prism. The B_3 moiety interacts with, and thereby form delocalized bonds with the Ge_{12} prism according to the ELF result. Localization domains shown in Figure 4, which are located in region between the B_3 and Ge_{12}, illustrate a delocalized bonding character. These localization domains are closer to the B centers illustrating the fact that electrons tend to be concentrated around the B_3 unit. On the other hand, NBO atomic charges of **3.A** agree with the ELF picture on the polar character of the bond. Although the $B_3Ge_{12}^+$ has a formal positive charge, each of three B atoms bears a negative net charge of −1.5 electron. This result confirms a polar bonding between the B_3 and Ge_{12} moieties arising from a great charge transfer from Ge_{12} to B_3. The $B_3Ge_{12}^+$ cluster can again be regarded as a $[B_3^{\delta-}\ Ge_{12}^{\delta+}]$ donor−acceptor complex.

A similar characteristic is also identified for B_4Ge_{12} **4.A** in which four B atoms prefer to connect together and act as a B_4 block. As indicated in Table 1, the MBO values performed for B_4 unit of **4.A** and free B_4 are nearly identical, being equal to ∼0.5. The ELF map of **4.A** (Figure 4) gives a similar observation. In fact the ELF map of **4.A** reveals the V(B,B,B,B) basin populated over four B atoms illustrating the formation of a four-center bond. Similar to the cases of $B_3Ge_{12}^+$ and B_2Ge_{12}, the B_4 cycle in **4.A** also brings in a strongly delocalized bonding with the Ge_{12} moiety, in constructing the hexagonal tubular prism. Actually, localization domains appeared in the region between both B_4 unit and Ge_{12} prism is associated with the emergence of delocalized bond between the B_4 dopant with the Ge_{12} host. In terms of charge transfer, the Ge_{12} host again supplies its electrons to the B_4 moiety, in such a way that each B atom bears a negative net charge of −1.3 electron, emphasizing again the importance of induced electrostatic interaction within an apparent $[B_4^{\delta-}\ Ge_{12}^{\delta+}]$ donor−acceptor complex.

In summary, the above analysis gives an emphasis that the small B_2, B_3, and B_4 clusters can be used as efficient dopants to turn Ge hosts into high symmetry clusters. Boron atoms introduced into a Ge_{12} host maintain both geometric and bonding characteristics as in free B_2, B_3, and B_4 clusters according to calculated ELF and MBO results. These small B clusters connect with Ge_{12} host through delocalized bonds. The Ge_{12} host carries out a great charge transfer to B_x and thereby produces a kind of $[B_x^{\delta-}\ Ge_{12}^{\delta+}]$ donor−acceptor complex. The B_x units can be considered as negatively charged islands surrounded in positively charged Ge_{12} tubes.

3.5. Molecular Orbital Interactions between Ge_{12} and B_x Units. The special geometries of B_2Ge_{12}, $B_3Ge_{12}^+$, and B_4Ge_{12} clusters deserve a further analysis in order to more deeply understand the stabilizing interactions as well as the inherent electronic requirements. Orbital interaction diagrams between B_x dopants and their respective Ge_{12} skeletons are constructed and displayed in Figures 5−7. The orbital shapes of **2.A**, **3.A**, and **4.A** structures associating to orbital interaction between B_x and Ge_{12} are given in Figures S6−S8 of Supporting Information file. For the smallest germanium deltahedron, orbital interactions of the B_2 dimer with the deltahedral Ge_{12} emphasize an interesting perspective on its stability. As displayed in Figure 5, the doubly occupied molecular orbitals (MOs) of the Ge_{12} host involving the $5a_g$ and $4a_g$ MOs enjoy stabilizing interactions with the $2\pi_u$ of B_2 and subsequently establish the fully occupied $5a_g$, $6a_g$, and $7a_g$ levels for B_2Ge_{12} **2.A**.

Similarly, the $2b_{2g}$ MO of B_2Ge_{12} **2.A** is constructed by combination of the $2b_{2g}$ level of Ge_{12} and $2\pi_g$ of B_2, whereas the $1\pi_g$ of B_2 enjoys an interaction with the $3b_{1g}$ eigenstate of Ge_{12} host and generate the $2b_{1g}$ MO of B_4Ge_{12}, which is occupied by two electrons. The $2\sigma_g$ vacant level of B_2 is an orbital overlap with $4b_{2u}$ eigenstate of Ge_{12}, which is occupied by two electrons, and produces subsequently the doubly occupied $3b_{2u}$ MO of B_2Ge_{12}. These interactions are associated with an electron donation from Ge_{12} to B_2 and give rise to an enhanced stability for the resulting B_2Ge_{12}. This finding is in agreement with NBO calculations discussed above.

Orbital interaction diagrams also reveal another special bonding feature of the B_2Ge_{12} deltahedron. The B_2 highest

DOI: 10.1021/acs.jpcc.9b05483
J. Phys. Chem. C 2019, 123, 24676−24684

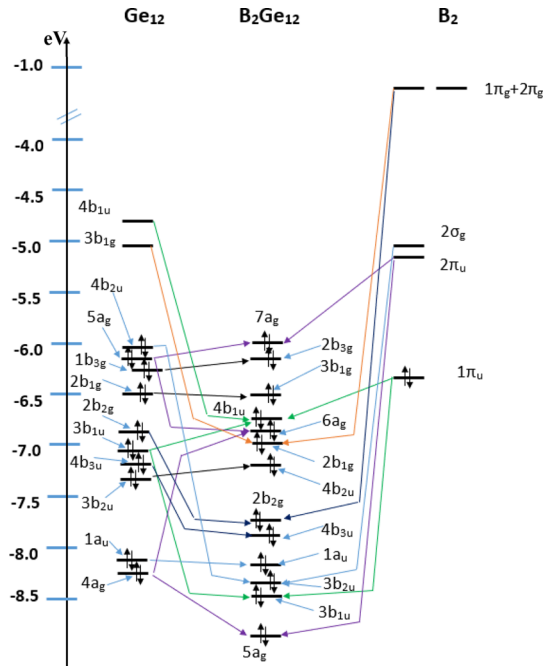

Figure 5. Orbital interaction diagram of B_2 and Ge_{12} in D_{2h} symmetry forming the **2.A** structure. The eigenvalues were obtained by TPSSh/6-311+G(d) calculations.

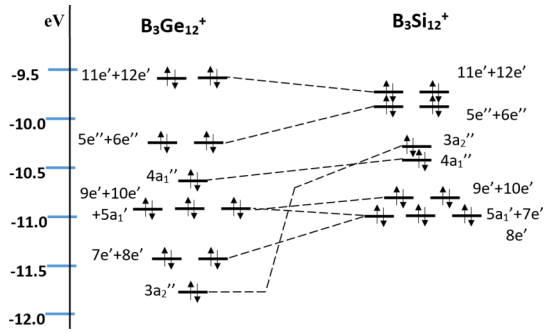

Figure 6. Quantitative correlation diagram between $B_3Ge_{12}^+$ and $B_3Si_{12}^+$ clusters. The eigenvalues were obtained by the TPSSh/6-311+G(d) calculations.

occupied MO (HOMO) is involved in an interaction with the fully occupied $3b_{1u}$ and empty $4b_{1u}$ MOs of Ge_{12}, and subsequently induce two fully occupied MOs, namely, $3b_{1u}$ and $4b_{1u}$, for D_{2h} B_2Ge_{12} **2.A**. As a result, the stability of B_2Ge_{12} is also contributed by electron backdonation from the B_2 unit.

Regarding the $B_3Ge_{12}^+$ hexagonal prism **3.A**, an orbital interaction diagram between the D_{3h} B_3^+ and Ge_{12} skeleton is constructed and shown in Figure S5 of the Supporting Information file. Because of the fact that both isovalent $B_3Ge_{12}^+$ and $B_3Si_{12}^+$ clusters exhibit the same type of geometry,[36] it is meaningful to comparatively explore their electronic structure, and identify the stabilizing effect of the B_3 dopant. Empty delocalized MOs of B_3^+ gain electrons from the Ge_{12} moiety through orbital overlap, and subsequently give rise a strong stability for the $B_3Ge_{12}^+$ cluster.

Actually, six empty levels of B_3^+ including lowest unoccupied MO (LUMO) (a_1'), LUMO + 1,1′ (e′) and LUMO + 2,2′ (e″) enjoy stabilizing interactions with LUMO and LUMO + 1,1′ of Ge_{12}, and consequently induce thermodynamic stability for the resulting $B_3Ge_{12}^+$ hexagonal prism. Quite similar to $B_3Si_{12}^+$, the

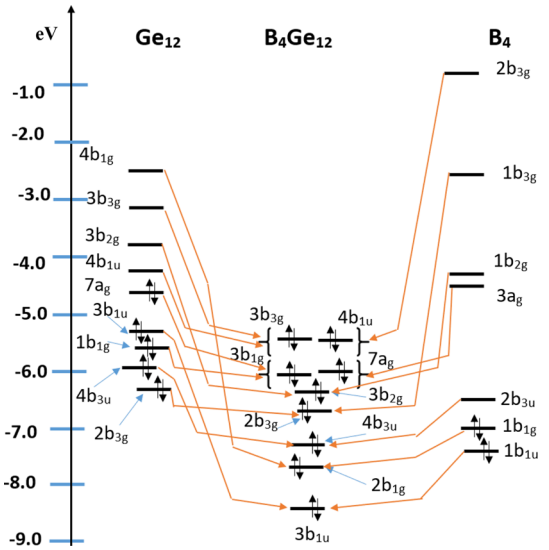

Figure 7. Orbital interaction diagram of B_4 and Ge_{12} in D_{2h} symmetry forming **4.A** structure. The eigenvalues were obtained by TPSSh/6-311+G(d) calculations.

stability of $B_3Ge_{12}^+$ is enhanced by the interaction of bonding MOs of the B_3^+ unit with Ge_{12}. As displayed in Figure S5 (Supporting Information), three bonding $1a_2''$ and 2e′ + 3e′ levels of B_3^+ are actually involved in an orbital overlap with the HOMO − 1 (a_2'') and HOMO − 4,4′ (e′) of D_{3h} Ge_{12}. These interactions subsequently generate the $3a_2''$ and 9e′ + 10e′ eigenstates and thereby give rise to the stable $B_3Ge_{12}^+$ cluster in the high D_{3h} symmetry. Figure 4 displays a qualitative correlation between both $B_3Si_{12}^+$ and $B_3Ge_{12}^+$ clusters in terms of eigenstates. Hence, through orbital interactions with Ge_{12} and Si_{12} tubular skeletons, both empty and occupied MOs of the B_3^+ cycle are strongly stabilized and thereby produce the stabilized D_{3h} $B_3Ge_{12}^+$ and $B_3Si_{12}^+$ tubes.

Orbital interaction diagram of both B_4 and Ge_{12} units in D_{2h} symmetry is now explored to understand how a B_4 cycle actually stabilizes a Ge_{12} block into a D_{2h} shape. It is illustrative that both B_4Ge_{12} and $B_3Ge_{12}^+$ hexagonal prisms share a similar stabilizing mechanism in which both empty and occupied MOs of the B_4 unit are stabilized. The B_4 cycle receives an electron donation from the Ge_{12} host through the orbital overlap. The $1b_{3g}$, $3a_g$, and $2b_{3u}$ empty levels of the B_4 cycle are involved in stabilizing interactions with the doubly occupied $2b_{3g}$, $7a_g$, and $4b_{3u}$ MOs of Ge_{12}, and subsequently produce the $7a_g$, $2b_{3g}$, and $4b_{3u}$ eigenstates, which are fulfilled by 6 electrons, of the D_{2h} B_4Ge_{12} tubular structure **4.A**. These interactions emphasize that a fulfilment of empty MOs of B_4 plays an essential factor for the stabilization of the binary B_4Ge_{12} cluster in a D_{2h} shape.

Orbital interactions also indicate another important contributor to the stabilizing mechanism where empty levels of the D_{2h} Ge_{12} tube are important. As shown in Figure 7, orbital overlaps of the $4b_{1g}$, $3b_{2g}$, and $3b_{1u}$ MOs of Ge_{12} with the $1b_{1g}$, $1b_{2g}$, and $1b_{1u}$ MOs of B_4 tend to stabilize the B_4Ge_{12} tubular cluster. These interactions give rise to the doubly occupied $3b_{2g}$, $2b_{1g}$, and $3b_{1u}$ MOs for B_4Ge_{12}. Therefore, occupancy of the empty levels of the Ge_{12} skeleton as well as reinforcement of bonding MOs of the B_4 cycle constitute important contributors to the thermodynamic stability of the B_4Ge_{12} hexagonal prism **4.A**.

The abovementioned analysis on bonding trends points out a general perspective on an electronic requirement for the

DOI: 10.1021/acs.jpcc.9b05483
J. Phys. Chem. C 2019, 123, 24676−24684

formation of the tubular geometry. Establishment of delocalized bonds between the B_x^q dopant and the Ge_{12} skeletons ends up in an enhanced stability for the doped $B_xGe_{12}^q$ clusters. The transition metal-doped MGe_{12}^q clusters also share such a stabilization mechanism. Depending on the dopant characteristics, MGe_{12}^q structures actually tend to favor a puckered hexagonal prism, bicapped pentagonal prism, or icosahedral geometry. Investigation on the correlationship between geometry and bonding suggests that a maximization of electron density overlaps between the Ge_{12} cage and metal dopant is a driving force for formation of MGe_{12}^q in different geometries.[58] Although each B_x dopant basically generates a different geometry with a Ge_{12} host, they attain in all cases a stabilized electronic structure which is contributed by highly delocalized bonds made through strong orbital interactions.

A general principle to design tubular clusters can thus be proposed upon comparison to other tubular clusters. The M_2Si_{12} hexagonal prism,[59] Mn_2Si_{15} triple ring,[60] M_2B_{14} double ring,[61] and the Rh_2B_{18} teetotum[62] all have the most stable form in tubular geometry and such an enhanced stability is contributed by two main effects. The first effect is that both antibonding and bonding MOs of M_2 are stabilized through orbital interactions with delocalized eigenstates of the corresponding tube. The second factor is that the vacant eigenstate of the Si_{12}, Si_{15}, B_{14}, and B_{18} tubes becomes occupied in the resulting M_2Si_{12}, Mn_2Si_{15}, M_2B_{14}, and Rh_2B_{18} structure, respectively, and this also contributes to a stabilization of the latter. It is clear that the M_2 and B_x dopants induce the delocalized bond with either Ge, Si, or B hosts to generate the tubular frames. Hence, an electronic principle for formation of tubular clusters is that the dopants are able to generate delocalized bonds with their host in a tubular shape, and subsequently attain a high-symmetry stable configuration.

3.6. Aromaticity of $B_3Ge_{12}^+$ and B_4Ge_{12} Clusters. With the appearance of delocalized bonds, it is insightful to further explore the aromatic features of both $B_3Ge_{12}^+$ and B_4Ge_{12} tubular prisms. Previous reports indicated that aromaticity constitutes a main reason for the planar shape of boron-based clusters.[63] Because it is rather difficult to classify the MOs of either $B_3Ge_{12}^+$ or B_4Ge_{12} into different σ and π sets, we now explore their magnetic ring current maps with respect to three different planes. The first plane contains either the B_3 or B_4 cycle, denoted as P_0 plane. The second plane is located about 1 a.u. above the P_0 plane, called P_1 plane. Finally, the third plane involves a Ge_6 hexagon and named as P_2 plane. Exploration of the ring current density projected into these planes, in particular the P_1 plane, provides us with an intrinsic aromatic character of these novel type of clusters. The total magnetic ring current maps of $B_3Ge_{12}^+$ **3.A** and B_4Ge_{12} **4.A** that are projected onto the P_0, P_1, and P_2 planes are displayed in Figure 8.

Regarding both P_0 and P_1 planes, both $B_3Ge_{12}^+$ and B_4Ge_{12} sustain diatropic ring current flows induced by an external magnetic field, thus indicating a certain aromatic character for these tubular clusters. For both free B_3 and B_4 cycles, appearance of diatropic induced current densities in both P_0 and P_1 planes shows both σ and π aromatic characters, respectively. However, because of the involvement of MOs of Ge_{12} skeletons in $B_3Ge_{12}^+$ and B_4Ge_{12}, the total ring current maps projected into P_0 and P_1 planes cannot separately be considered as σ and π contributions. Diatropic current density flows are identified in the P_2-plane indicating an aromatic

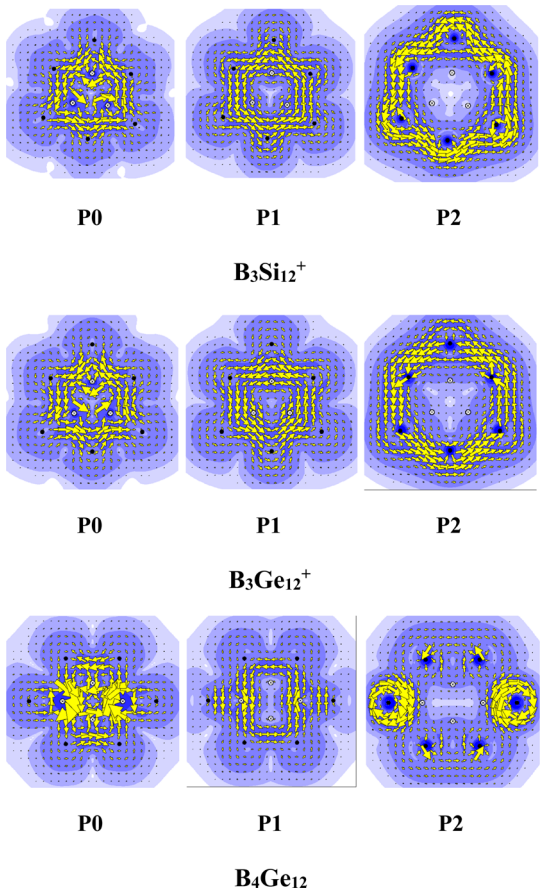

Figure 8. Comparison of the magnetic ring current maps of $B_3Si_{12}^+$, $B_3Ge_{12}^+$ **3.A** and B_4Ge_{12} **4.A** in different planes. P_0 is the plane containing B_3 or B_4 cycle, P_1 is the plane 1 a.u above P_0, and P_2 is the plane containing a Ge_6 face. Ring current maps were obtained from B3P86/6-311+G(d) electron densities.

feature of the Ge_6 hexagon. It is illustrative that diatropic ring currents for both $B_3Ge_{12}^+$ and B_4Ge_{12} are not only discernible on the B_3 and B_4 cycles but also on the hexagonal face of the Ge_{12} skeleton. This result emphasizes that the aromatic character of both tubular clusters $B_3Ge_{12}^+$ and B_4Ge_{12} is not solely contributed by the B_3 and B_4 dopants, but the Ge_{12} tubular skeleton equally has an important role. Indeed, the D_{2h} Ge_{12} skeleton and B_4 dopant of B_4Ge_{12} each separately show a strongly paratropic current density associating with an anti-aromatic feature. Combination of both moieties end up with a high-symmetry stable aromatic cluster, clearly indicating that aromaticity plays a more crucial role in the design principle of tubular clusters. It is related to orbital interactions leading to formation of delocalized bonds, that are regarded, as discussed above, to be a driving force in stabilizing tubular clusters. The magnetic ring current calculations suggest that aromaticity, which is resulting from electron delocalization, constitutes another essential factor in the stabilization mechanism.

4. CONCLUDING REMARKS

In the present theoretical study, we successfully designed the boron-doped germanium $B_xGe_{12}^q$ clusters with $x = 1, 2, 3$, and 4 and $q = 0, 1$. While the B_2Ge_{12} structure constitutes the smallest deltahedral germanium cluster, both $B_3Ge_{12}^+$ and B_4Ge_{12} clusters present us, for the first time, with an endohedral tubular motif where either the B_3 or the B_4 cycle

DOI: 10.1021/acs.jpcc.9b05483
J. Phys. Chem. C 2019, 123, 24676−24684

is essentially encapsulated by a Ge_{12} hexagonal prism. Both B_3 and B_4 units satisfy a geometry requirement to establish endohedral structures within a Ge_{12} host.

Within D_{3h} and D_{2h} geometries, the B_3 and B_4 clusters generate delocalized bonds with the Ge_{12} framework and thereby induce an aromatic character for the resulting $B_3Ge_{12}^+$ and B_4Ge_{12}. Such a tubular aromaticity appears to greatly contribute to the high thermodynamic stability of the binary hexagonal Ge tubes. Together, both characteristics constitute a design electronic principle for making stabilized tubular clusters.

■ ASSOCIATED CONTENT

Supporting Information

The Supporting Information is available free of charge on the ACS Publications website at DOI: 10.1021/acs.jpcc.9b05483.

Geometrical shapes of lower-lying isomers of the $[B_xGe_{12}]^{0/+}$ and B_4Si_{12} and their relative energies, the MO shapes of **2.A**, **3.A**, and **4.A**, orbital interaction diagram of $[B_3Ge_{12}]^+$, and Cartesian coordinates of the optimized ground-state structures of $[B_xGe_{12}]^{0/+}$ (PDF)

■ AUTHOR INFORMATION

Corresponding Author

*E-mail: nguyenminhtho@tdtu.edu.vn.

ORCID

Hung Tan Pham: 0000-0001-6356-3167

Remco W. A. Havenith: 0000-0003-0038-6030

Minh Tho Nguyen: 0000-0002-3803-0569

Notes

The authors declare no competing financial interest.

■ ACKNOWLEDGMENTS

H.T.P. and M.T.N. are grateful to the Department of Science and Technology, Ho Chi Minh City, Vietnam, for support under Grant nos. 414/QĐ-KHCNTT & 1398/QĐ-SKHCN.

■ REFERENCES

(1) Kamata, Y. High-k/Ge MOSFETs for Future Nanoelectronics. *Mater. Today* **2008**, *11*, 30−38.

(2) Pillarisetty, R. Academic and industry research progress in germanium nanodevices. *Nature* **2011**, *479*, 324−328.

(3) Wang, J.; Wang, G.; Zhao, J. Structure and Electronic Properties of Ge_n (n = 2−25) Clusters from Density-functional Theory. *Phys. Rev. B: Condens. Matter Mater. Phys.* **2001**, *64*, 205411.

(4) King, R. B.; Silaghi-Dumitrescu, I.; Lupan, A. Density Functional Theory Study of 11-Atom Germanium Clusters: Effect of Electron Count on Cluster Geometry. *Inorg. Chem.* **2005**, *44*, 3579−3588.

(5) King, R. B.; Silaghi-Dumitrescu, I.; Uţă, M. M. Density Functional Theory Study of 10-Atom Germanium Clusters: Effect of Electron Count on Cluster Geometry. *Inorg. Chem.* **2006**, *45*, 4974−4981.

(6) King, R. B.; Silaghi-Dumitrescu, I. Density Functional Theory Study of Nine-Atom Germanium Clusters: Effect of Electron Count on Cluster Geometry. *Inorg. Chem.* **2003**, *42*, 6701−6708.

(7) Qin, W.; Lu, W.-C.; Zang, Q.-J.; Zhao, L.-Z.; Chen, G.-J.; Wang, C. Z.; Ho, K. M. Geometric structures of Gen (n = 34-39) clusters. *J. Chem. Phys.* **2010**, *132*, 214509.

(8) Qin, W.; Lu, W.-C.; Zhao, L.-Z.; Zang, Q.-J.; Chen, G.-J.; Wang, C. Z.; Ho, K. M. Platelike structures of semiconductor clusters Gen (n = 40-44). *J. Chem. Phys.* **2009**, *131*, 124507.

(9) Li, B.-x.; Cao, P.-l. Structures ofGenclusters (n = 3-10) and comparisons toSi_n clusters. *Phys. Rev. B: Condens. Matter Mater. Phys.* **2000**, *62*, 15788−15796.

(10) Shvartsburg, A. A.; Liu, B.; Lu, Z.-Y.; Wang, C.-Z.; Jarrold, M. F.; Ho, K.-M. Structures of Germanium Clusters: Where the Growth Patterns of Silicon and Germanium Clusters Diverge. *Phys. Rev. Lett.* **1999**, *83*, 2167.

(11) Wang, L.; Zhao, J. Competition between supercluster and stuffed cage structures in medium-sized Gen (n = 30-39) clusters. *J. Chem. Phys.* **2008**, *128*, 024302.

(12) Bulusu, S.; Yoo, S.; Zeng, X. C. Search for global minimum geometries for medium sized germanium clusters: Ge12−Ge20. *J. Chem. Phys.* **2005**, *122*, 164305.

(13) Yoo, S.; Zeng, X. C. Search for global-minimum geometries of medium-sized germanium clusters. II. Motif-based low-lying clusters Ge21−Ge29. *J. Chem. Phys.* **2006**, *124*, 184309.

(14) Spiekermann, A.; Hoffmann, S. D.; Kraus, F.; Fässler, T. F. $[Au_3Ge_{18}]^{5-}$—A Gold−Germanium Cluster with Remarkable Au−Au Interactions. *Angew. Chem., Int. Ed.* **2007**, *46*, 1638−1640.

(15) Perla, L. G.; Muñoz-Castro, A.; Sevov, S. C. Eclipsed- and Staggered-$[Ge_{18}Pd_3\{E^iPr_3\}_6]^{2-}$ (E = Si, Sn): Positional Isomerism in Deltahedral Zintl Clusters. *J. Am. Chem. Soc.* **2017**, *139*, 15176−15181.

(16) Perla, L. G.; Sevov, S. C. A Stannyl-Decorated Zintl Ion $[Ge_{18}Pd_3(Sn^iPr_3)_6]^{2-}$: Twinned Icosahedron with a Common Pd_3-Face or 18-Vertex *Hypho*-Deltahedron with a Pd_3-Triangle Inside. *J. Am. Chem. Soc.* **2016**, *138*, 9795−9798.

(17) Goicoechea, J. M.; Sevov, S. C. $[(Pd−Pd)@Ge_{18}]^{4-}$: A Palladium Dimer Inside the Largest Single-Cage Deltahedron. *J. Am. Chem. Soc.* **2005**, *127*, 7676−7677.

(18) Liu, C.; Popov, I. A.; Li, L.-J.; Li, N.; Boldyrev, A. I.; Sun, Z.-M. $[Co_2@Ge_{16}]^{4-}$: Localized versus Delocalized Bonding in Two Isomeric Intermetalloid Clusters. *Chem.—Eur. J.* **2018**, *24*, 699−705.

(19) Jin, X.; Espinoza-Quintero, G.; Below, B.; Arcisauskaite, V.; Goicoechea, J. M.; McGrady, J. E. Structure and bonding in a bimetallic endohedral cage, $[Co_2@Ge_{16}]^{z-}$. *J. Organomet. Chem.* **2015**, *792*, 149−153.

(20) Zhou, B.; Denning, M. S.; Kays, D. L.; Goicoechea, J. M. Synthesis and Isolation of $[Fe@Ge_{10}]^{3-}$: A Pentagonal Prismatic Zintl Ion Cage Encapsulating an Interstitial Iron Atom. *J. Am. Chem. Soc.* **2009**, *131*, 2802−2803.

(21) Wang, J.-Q.; Stegmaier, S.; Fässler, T. F. $[Co@Ge_{10}]^{3-}$: An Intermetalloid Cluster with Archimedean Pentagonal Prismatic Structure. *Angew. Chem., Int. Ed.* **2009**, *48*, 1998−2002.

(22) Kumar, V.; Kawazoe, Y. Metal-Encapsulated Caged Clusters of Germanium with Large Gaps and Different Growth Behavior than Silicon. *Phys. Rev. Lett.* **2002**, *88*, 235504.

(23) Jing, Q.; Tian, F.-y.; Wang, Y.-x. No Quenching of Magnetic Moment for the Ge_nCo (n=1−13) Clusters: First-principles Calculations. *J. Chem. Phys.* **2008**, *128*, 124319.

(24) Deng, X.-J.; Kong, X.-Y.; Xu, X.-L.; Xu, H.-G.; Zheng, W.-J. Structural and Magnetic Properties of $CoGe_n^-$ (n=2−11) Clusters: Photoelectron Spectroscopy and Density Functional Calculations. *ChemPhysChem* **2014**, *15*, 3987−3993.

(25) Wang, J.; Han, J.-G. A Theoretical Study on Growth Patterns of Ni-Doped Germanium Clusters. *J. Phys. Chem. B* **2006**, *110*, 7820−7827.

(26) Deng, X.-J.; Kong, X.-Y.; Xu, H.-G.; Xu, X.-L.; Feng, G.; Zheng, W.-J. Photoelectron Spectroscopy and Density Functional Calculations of VGe_n^- (n = 3−12) Clusters. *J. Phys. Chem. C* **2015**, *119*, 11048−11055.

(27) Siouani, C.; Mahtout, S.; Safer, S.; Rabilloud, F. Structure, Stability, and Electronic and Magnetic Properties of VGe_n (n = 1−19) Clusters. *J. Phys. Chem. A* **2017**, *121*, 3540−3554.

(28) Hou, X.-J.; Gopakumar, G.; Lievens, P.; Nguyen, M. T. Chromium-Doped Germanium Clusters $CrGe_n$ (n = 1−5): Geometry, Electronic Structure, and Topology of Chemical Bonding. *J. Phys. Chem. A* **2007**, *111*, 13544−13553.

(29) Bandyopadhyay, D.; Kaur, P.; Sen, P. New Insights into Applicability of Electron-Counting Rules in Transition Metal Encapsulating Ge Cage Clusters. *J. Phys. Chem. A* **2010**, *114*, 12986−12991.

DOI: 10.1021/acs.jpcc.9b05483
J. Phys. Chem. C 2019, 123, 24676−24684

(30) Wang, J.; Han, J.-G. Geometries and Electronic Properties of the Tungsten-Doped Germanium Clusters: WGe_n (n = 1−17). *J. Phys. Chem. A* **2006**, *110*, 12670−12677.
(31) Trivedi, R.; Dhaka, K.; Bandyopadhyay, D. Study of Electronic Properties, Stabilities and Magnetic Quenching of Molybdenum-doped Germanium Clusters: a Density Functional Investigation. *RSC Adv.* **2014**, *4*, 64825−64834.
(32) Jin, Y.; Tian, Y.; Kuang, X.; Lu, C.; Cabellos, J. L.; Mondal, S.; Merino, G. Structural and Electronic Properties of Ruthenium-Doped Germanium Clusters. *J. Phys. Chem. C* **2016**, *120*, 8399−8404.
(33) Jaiswal, S.; Kumar, V. Growth Behavior and Electronic Structure of Neutral and Anion $ZrGe_n$ (n = 1−21) Clusters. *Comput. Theor. Chem.* **2016**, *1075*, 87−97.
(34) Phi, N. D.; Trung, N. T.; Ewald, J.; Ngan, V. T. Electron Counting Rules for Transition Metal-doped Si_{12} Clusters. *Chem. Phys. Lett.* **2016**, *643*, 103−108.
(35) Lu, S.-J.; Hu, L.-R.; Xu, X.-L.; Xu, H.-G.; Chen, H.; Zheng, W.-J. Transition from Exohedral to Endohedral Structures of $AuGe_n^-$ (n = 2−12) Clusters: Photoelectron Spectroscopy and ab initio Calculations. *Phys. Chem. Chem. Phys.* **2016**, *18*, 20321−20329.
(36) Pham, H. T.; Dang, T. T. M.; Van Duong, L.; Tam, N. M.; Nguyen, M. T. $B_3@Si_{12}^+$: Strong Stabilizing Effects of a Triatomic Cyclic Boron Unit on Tubular Silicon Clusters. *Phys. Chem. Chem. Phys.* **2018**, *20*, 7588.
(37) Koukaras, E. N. Ab initio study of medium sized boron-doped silicon clusters SinBm, n = 11−13, m = 1−3. *Phys. Chem. Chem. Phys.* **2018**, *20*, 18556−18570.
(38) Pham, H. T.; Duong, L. V.; Pham, B. Q.; Nguyen, M. T. The 2D-to-3D Geometry Hopping in Small Boron Clusters: The Charge Effect. *Chem. Phys. Lett.* **2013**, *577*, 32−37.
(39) Tao, J.; Perdew, J. P.; Staroverov, V. N.; Scuseria, G. E. Climbing the Density Functional Ladder: Nonempirical Meta−Generalized Gradient Approximation Designed for Molecules and Solids. *Phys. Rev. Lett.* **2003**, *91*, 146401.
(40) Becke, A. D. Density-functional thermochemistry. III. The role of exact exchange. *J. Chem. Phys.* **1993**, *98*, 5648−5652.
(41) Baek, H.; Moon, J.; Kim, J. Benchmark Study of Density Functional Theory for Neutral Gold Clusters, Au_n (n = 2−8). *J. Phys. Chem. A* **2017**, *121*, 2410−2419.
(42) Pham, H. T.; Duong, L. V.; Tam, N. M.; Pham-Ho, M. P.; Nguyen, M. T. The Boron Conundrum: Bonding in the Bowl B_{30} and B_{36}, Fullerene B_{40} and Triple Ring B_{42} Clusters. *Chem. Phys. Lett.* **2014**, *608*, 295−302.
(43) Gordon, M. S.; Binkley, J. S.; Pople, J. A.; Pietro, W. J.; Hehre, W. J. Self-consistent Molecular Orbital Methods. 22. Small Split-valence Basis Sets for Second-row Elements. *J. Am. Chem. Soc.* **1982**, *104*, 2797−2803.
(44) Dobbs, K. D.; Hehre, W. J. Molecular Orbital Theory of the Properties of Inorganic and Organometallic Compounds 5. Extended Basis Sets for First-row Transition Metals. *J. Comput. Chem.* **1987**, *8*, 861−879.
(45) Krishnan, R.; Binkley, J. S.; Seeger, R.; Pople, J. A. Self-consistent Molecular Orbital Methods. XX. A Basis Set for Correlated Wave Functions. *J. Chem. Phys.* **1980**, *72*, 650−660.
(46) Jeffrey Hay, P. Gaussian basis sets for molecular calculations. The representation of 3d orbitals in transition-metal atoms. *J. Chem. Phys.* **1977**, *66*, 4377−4384.
(47) Silvi, B.; Savin, A. Classification of Chemical Bonds Based on Topological Analysis of Electron Localization Functions. *Nature* **1994**, *371*, 683−686.
(48) Mayer, I. Bond Order and Valence Indices: A Personal Account. *J. Comput. Chem.* **2007**, *28*, 204−221.
(49) Reed, A. E.; Curtiss, L. A.; Weinhold, F. Intermolecular Interactions from a Natural Bond Orbital, Donor-Acceptor Viewpoint. *Chem. Rev.* **1988**, *88*, 899−926.
(50) Frisch, M. J.; Schlegel, H. B.; Scuseria, G. E.; Robb, M. A.; Cheeseman, J. R.; Montgomery, J. A.; Vreven, T.; Kudin, K. N.; Burant, J. C.; Millam, J.; et al. *Gaussian 09*, Revision B.01; Gaussian, Inc.: Wallingford, CT, 2009.
(51) Zanasi, R. Coupled Hartree-Fock calculations of molecular magnetic properties annihilating the transverse paramagnetic current density. *J. Chem. Phys.* **1996**, *105*, 1460−1469.
(52) Lazzeretti, P.; Malagoli, M.; Zanasi, R. Computational Approach to Molecular Magnetic Properties by Continuous Transformation of the Origin of the Current Density. *Chem. Phys. Lett.* **1994**, *220*, 299−304.
(53) Lazzeretti, P.; Malagoli, P. M.; Zanasi, R. R. *SYSMO package, Technical Report "Sistemi Informatici e Calcolo Parallelo", CNR Italy*, 1991. Research Report number 1/67. Additional Routines by Fowler, P. W.; Steiner, E.; Havenith, R. W. A. and Soncini, A.
(54) Havenith, R. W. A.; Fowler, P. W. Ipsocentric Ring Currents in Density Functional Theory. *Chem. Phys. Lett.* **2007**, *449*, 347−353.
(55) Guest, M. F.; et al. The GAMESS-UK electronic structure package: algorithms, developments and applications. *Mol. Phys.* **2005**, *103*, 719−747.
(56) Bruce King, R.; Silaghi-Dumitrescu, I.; Uţă, M. M. Density functional theory study of twelve-atom germanium clusters: conflict between the Wade-Mingos rules and optimum vertex degrees. *Dalton Trans.* **2007**, 364−372.
(57) Zhai, H.-J.; Wang, L.-S.; Alexandrova, A. N.; Boldyrev, A. I.; Zakrzewski, V. G. Photoelectron Spectroscopy and ab Initio Study of B_3^- and B_4^-Anions and Their Neutrals. *J. Phys. Chem. A* **2003**, *107*, 9319−9328.
(58) Goicoechea, J. M.; McGrady, J. E. On the Structural Landscape in Endohedral Silicon and Germanium Clusters, $M@Si_{12}$ and $M@Ge_{12}$. *Dalton Trans.* **2015**, *44*, 6755−6766.
(59) Pham, H. T.; Majumdar, D.; Leszczynski, J.; Nguyen, M. T. 4d and 5d Bimetal Doped Tubular Silicon Clusters Si12M2 with M = Nb, Ta, Mo and W: a Bimetallic Configuration Model. *Phys. Chem. Chem. Phys.* **2017**, *19*, 3115−3124.
(60) Pham, H. T.; Phan, T.-T.; Tam, N. M.; Duong, L. V.; Pham-Ho, M. P.; Nguyen, M. T. $Mn_2@Si_{15}$: the Smallest Triple Ring Tubular Silicon Cluster. *Phys. Chem. Chem. Phys.* **2015**, *17*, 17566−17570.
(61) Pham, H. T.; Nguyen, M. T. Effects of Bimetallic Doping on Small Cyclic and Tubular Boron Clusters: B_7M_2 and $B_{14}M_2$ Structures with M = Fe, Co. *Phys. Chem. Chem. Phys.* **2015**, *17*, 17335−17345.
(62) Pham, H. T.; Nguyen, M. T. Formation of a Bi-rhodium Boron Tube Rh_2B_{18} and its Great CO_2 Capture Ability. *Phys. Chem. Chem. Phys.* **2018**, *20*, 26072−26082.
(63) Pham, H. T.; Lim, K. Z.; Havenith, R. W. A.; Nguyen, M. T. Aromatic Character of Planar Boron-based Clusters Revisited by Ring Current Calculations. *Phys. Chem. Chem. Phys.* **2016**, *18*, 11919−11931.

DOI: 10.1021/acs.jpcc.9b05483
J. Phys. Chem. C 2019, 123, 24676−24684